\



Spin and spin-orbit coupling effects in nickel-based superalloys: A first-principles study on Ni_3Al doped with Ta/W/Re

Liping Liu(刘立平), Jin Cao(曹晋), Wei Guo(郭伟), and Chongyu Wang(王崇愚)
Citation: Chin. Phys. B, 2022, 31 (**1**): 016105. DOI: 10.1088/1674-1056/ac4024
Journal homepage: http://cpb.iphy.ac.cn; http://iopscience.iop.org/cpb

What follows is a list of articles you may be interested in

Doping effect on the structure and physical properties of quasi-one-dimensional compounds $Ba_9Co_3(Se_{1-x}S_x)_{15}$ (x = 0-0.2)

Lei Duan(段磊), Xian-Cheng Wang(望贤成), Jun Zhang(张俊), Jian-Fa Zhao(赵建发), Wen-Min Li(李文敏), Li-Peng Cao(曹立朋), Zhi-Wei Zhao(赵志伟), Changjiang Xiao(肖长江), Ying Ren(任瑛), Shun Wang(王顺), Jinlong Zhu(朱金龙), and Chang-Qing Jin(靳常青)
Chin. Phys. B, 2021, 30 (**10**): 106101. DOI: 10.1088/1674-1056/ac1f03

Strain-tuned magnetic properties in (Ga,Fe)Sb: First-principles study

Feng-Chun Pan(潘凤春), Xue-Ling Lin(林雪玲), and Xu-Ming Wang(王旭明)
Chin. Phys. B, 2021, 30 (**9**): 096105. DOI: 10.1088/1674-1056/ac00a2

X-ray absorption investigation of the site occupancies of the copper element in nominal $Cu_3Zn(OH)_6FBr$

Ruitang Wang(王瑞塘), Xiaoting Li(李效亭), Xin Han(韩鑫), Jiaqi Lin(林佳琪), Yong Wang(王勇), Tian Qian(钱天), Hong Ding(丁洪), Youguo Shi(石友国), and Xuerong Liu(柳学榕)
Chin. Phys. B, 2021, 30 (**4**): 046102. DOI: 10.1088/1674-1056/abe0c8

Electronic structure & yield strength prediction for dislocation–Mo complex in the γ phase of nickel-based superalloys

Feng-Hua Liu(刘凤华), Chong-Yu Wang(王崇愚)
Chin. Phys. B, 2017, 26 (**7**): 076104. DOI: 10.1088/1674-1056/26/7/076104

Effect of H impurity on misfit dislocation in Ni-based single-crystal superalloy: molecular dynamic simulations

Yu Tao,Xie Hong-Xian,Wang Chong-Yu
Chin. Phys. B, 2012, 21 (**2**): 026104. DOI: 10.1088/1674-1056/21/2/026104

Spin and spin–orbit coupling effects in nickel-based superalloys: A first-principles study on Ni_3Al doped with Ta/W/Re

Liping Liu(刘立平)[1], Jin Cao(曹晋)[1], Wei Guo(郭伟)[1,†], and Chongyu Wang(王崇愚)[2,‡]

[1] *Key Laboratory of Advanced Optoelectronic Quantum Architecture and Measurement (MOE), School of Physics, Beijing Institute of Technology, Beijing* 100081, *China*

[2] *Department of Physics, Tsinghua University, Beijing* 100084, *China*

(Received 16 November 2021; revised manuscript received 1 December 2021; accepted manuscript online 5 December 2021)

Heavy elements (X = Ta/W/Re) play an important role in the performance of superalloys, which enhance the strength, anti-oxidation, creep resistance, and anti-corrosiveness of alloy materials in a high-temperature environment. In the present research, the heavy element doping effects in FCC-Ni(γ) and Ni_3Al(γ') systems are investigated in terms of their thermodynamic and mechanical properties, as well as electronic structures. The lattice constant, bulk modulus, elastic constant, and dopant formation energy in non-spin, spin polarized, and spin–orbit coupling (SOC) calculations are compared. The results show that the SOC effects are important in accurate electronic structure calculations for alloys with heavy elements. We find that including spin for both γ and γ' phases is necessary and sufficient for most cases, but the dopant formation energy is sensitive to different spin effects, for instance, in the absence of SOC, even spin-polarized calculations give 1% to 9% variance in the dopant formation energy in our model. Electronic structures calculations indicate that spin polarization causes a split in the metal d states, and SOC introduces a variance in the spin-up and spin-down states of the d states of heavy metals and reduces the magnetic moment of the system.

Keywords: nickel-based superalloys, Ni_3Al, spin, spin–orbit coupling, mechanical properties, electronic structures

PACS: 61.66.Dk, 61.82.Bg **DOI:** 10.1088/1674-1056/ac4024

1. Introduction

Recent years have seen the widespread usage of superalloys in turbine engines.[1,2] With excellent creep strength, good oxidation resistance, and good ductility,[3] nickel-based superalloys, i.e., FCC-Ni(γ) and Ni_3Al(γ'), have become popular in the aerospace industry since they have better mechanical properties after doping with certain chemical elements.[4,5] For instance, heavy elements such as Ta, W, and Re are widely used in nickel-based superalloys. The distributions of heavy elements significantly affect the microstructure of the superalloys and are crucial to the performance of nickel-based superalloys.

Many experiments were undertaken to understand the mechanical properties,[6–9] as well as the locations and diffusion of Ta,[10–12] W,[13,14] and Re[15,16] in superalloys. Ta and Re atoms prefer to substitute Al sites in γ' phase, while W atoms show no preference and can appear in both γ and Al sites in γ' phases.[14] Doping methods have been applied in superalloys to increase their ductility.[17] However, it is difficult to prepare a high-quality, heavy-element-doped superalloy, and it can be challenging to locate the optimal position of the heavy metal atoms in such a superalloy given its complicated microstructures. Theoretical simulations are helpful in decreasing the cost of superalloy studies. There are some theoretical calculations explaining the experiments,[10] showing where heavy elements prefer to reside,[18,19] and the reason why γ and γ' phases with chemical defects have good mechanical properties.[20–23] The mechanism of solid solution strength in superalloys remains elusive since accurate simulations with numerous species of heavily metallic elements (typically with ten species) are difficult. Moreover, considering the spin degree of freedom in simulations of systems with hundreds of metallic atoms is computationally demanding, and the spin–orbit coupling (SOC) effect is rather challenging for systems with hundreds of atoms. It is difficult to describe the magnetism of Ni_3Al due to spin-flucuations.[24] Although Ni_3Al is a weak ferromagnet and has a low Curie temperature (41 K), doping 5d elements may introduce local moments in the crystal and exibite different magnetic properties, especially when the alloys are produced and cooled to room temperature. For heavy atoms, the SOC effects can yield a large difference in predictions of likely electronic structures. Up to now, the SOC effects are rarely considered in published work related to superalloys. Importantly, systemic investigation of the roles played by spin and SOC in determining the lattice constant, space group symmetry, dopant formation energy, as well as magnetic and mechanical properties, is warranted, especially in Ni-based superalloys.

In the present research, by performing first-principles calculations, we have systematically calculated the lattice constant, formation energy, mechanical properties, and electronic

†Corresponding author. E-mail: weiguo7@bit.edu.cn

‡Corresponding author. E-mail: cywang@mail.tsinghua.edu.cn

© 2022 Chinese Physical Society and IOP Publishing Ltd

structures considering spin and SOC effects in FCC-Ni(γ) and Ni_3Al(γ') and their Ta, W, and Re-doped alloys, then compared them with non-spin polarized results. We found that including spin for both γ and γ' phases is necessary and sufficient in most cases, except that dopant formation energy is sensitive to different spin effects; even spin-polarized calculations give 1% to 9% variance compared to SOC at a doping density of 1/32.

2. Method and model

First-principles calculations were performed by using Vienna *ab-initio* simulation package (VASP) with projector-augmented-wave (PAW) potentials.[25–27] The exchange–correlation interactions are treated within the generalized gradient approximation (GGA) in the scheme of the Perdew–Burke–Ernzerhof (PBE) functional.[28] The energy cut-off for plane-wave basis is set to 400 eV. The Brillouin zone is sampled by a uniformed grid ($9\times9\times9$) for the unit cell of Ni_3Al, and the grid density is kept fixed in supercell calculations. First-order Methfessel–Paxton smearing is used in self-consistent field calculations.[29]

The SOC effect is derived from the relativistic Dirac equation under the low-velocity approximation, where SOC term can be written as

$$H_{\rm so} = \frac{\mathrm{i}\boldsymbol{\sigma}\cdot\boldsymbol{p}\times[\boldsymbol{p},V]}{4m^2c^2} = \frac{\mathrm{i}\boldsymbol{\sigma}\cdot\boldsymbol{p}\times(-\mathrm{i}\hbar\boldsymbol{\nabla}V)}{4m^2c^2} = \frac{\hbar}{4m^2c^2}(\boldsymbol{\nabla}V\times\boldsymbol{p})\cdot\boldsymbol{\sigma},$$

it implies the spin–orbital-coupling effect. In this work, the SOC term is taken into account in VASP with the spherical symmetry approximation[30]

$$V = -\frac{Ze^2}{r},$$

and the SOC term becomes

$$H_{\rm so} = \frac{Ze^2}{2m^2c^2r^3}\boldsymbol{L}\cdot\mathbf{S},$$

moreover, the expected value of $\boldsymbol{L}\cdot\boldsymbol{S}/r^3$ is[31]

$$\left\langle\frac{\boldsymbol{L}\cdot\boldsymbol{S}}{r^3}\right\rangle = \frac{Z^3\hbar^2[j(j+1)-l(l+1)-\frac{3}{4}]}{a_0^3n^3l(l+1)(2l+1)},$$

where a_0 is the Bohr radius, Z represents the number of nuclear charges, n is the main quantum number, l is the angular quantum number, and j is the total angular quantum number ($\boldsymbol{J}=\boldsymbol{L}+\boldsymbol{S}$). So, in the spherical symmetry approximation, the SOC strength is proportional to Z^4. As a result, heavy elements with large Z show strong SOC effects. The inversion and the time reversal symmetries of the Ni_3Al system with doping atoms are broken. It will induce a Zeeman splitting, and, the energy scale of this splitting is governed by the SOC strength. Given the heavy doping atom, it suggests that a pure non-spin calculation is inappropriate for such systems.

The conjugate gradient (CG) algorithm is used for structural relaxation. Volumes and bulk modulus can be calculated using Rose–Vinet[32] and Birch–Murnaghan[33,34] equations of states. In this work, the Birch–Murnaghan equations of states are used to optimize the volumes and calculate the bulk modulus of the structures:[34] these were processed by the Atomic Simulation Environment (ASE) package.[35] Forces on each atom are relaxed with a convergence criterion of 0.01 eV/Å.

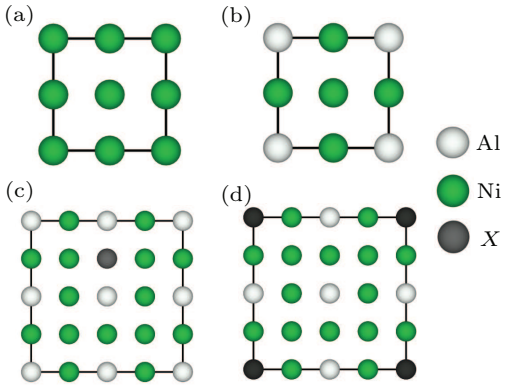


Fig. 1. (a) Ni(γ) unit cell (b) Ni_3Al(γ') unit cell; (c) $2\times2\times2$ supercell of Ni_3Al, and one of the Ni atoms is substituted by a doping atom X, where X = Ta, W, or Re; (d) $2\times2\times2$ supercell of Ni_3Al, and one Al is substituted by a doping atom X.

The strain tensor can be written in the following form:

$$\begin{pmatrix} e_{11} & e_{12} & e_{13} \\ e_{21} & e_{22} & e_{23} \\ e_{31} & e_{32} & e_{33} \end{pmatrix} = \begin{pmatrix} \varepsilon_1 & \frac{1}{2}\varepsilon_6 & \frac{1}{2}\varepsilon_5 \\ \frac{1}{2}\varepsilon_6 & \varepsilon_2 & \frac{1}{2}\varepsilon_4 \\ \frac{1}{2}\varepsilon_5 & \frac{1}{2}\varepsilon_4 & \varepsilon_3 \end{pmatrix}$$

and the total energy with strain ε_1, ε_2, ε_3, ε_4, ε_5, ε_6 is given by[36]

$$E(V,\{\varepsilon_i\}) = E(V_0,0) + \frac{1}{2}V_0\sum_{i,j=1}^{6}C_{ij}\varepsilon_i\varepsilon_j + \cdots,$$

where C_{ij} denotes the elastic constants, as calculated by use of the second-order derivative of total energy,[37,38] $E(V,\{\varepsilon_i\})$ and $E(V_0,0)$ are the total energy with and without strain, respectively, and V_0 represents the volume at equilibrium state. Five different strains from -1.0% to 1.0% are applied to the structures to fit the E–ε curve. The formation energy calculation is based on the Wagner–Schottky model,[39] as stated below (a more negative value means more energy-favorable), and all total energies are calculated using the same parameters and k-mesh density:

$$\Delta E(X_{\rm Ni}) = E_{\rm defect} + E_{\rm Ni} - E_{\rm perfect} - E_{{\rm solute}X},$$
$$\Delta E(X_{\rm Al}) = E_{\rm defect} + E_{\rm Al} - E_{\rm perfect} - E_{{\rm solute}X}.$$

Python Materials Genomics (pymatgen)[40] and vaspkit[41] are used to post-process electronic structure calculations. The

unit cells of FCC-Ni(γ) and Ni_3Al(γ') are shown in Figs. 1(a) and 1(b). Considering the fact that the doped heavy metal in Ni_3Al is a few percent in mole fraction in experiment, we have used a $2\times2\times2$ Ni_3Al supercell to simulate a heavy atom substitutional defect by replacing Ni/Al atom with an X (X = Ta/W/Re) atom as illustrated in Figs. 1(c) and 1(d).

3. Results

For models containing heavy atoms of Ta/W/Re, we treat SOC results as "correct", and compare results with non-spin and spin-polarization with SOC systematicallly in lattice constant, bulk modulus, elastic constant, dopant formation energy and electronic structures. As shown in supplementary material Table S1, our calculated lattice constant, bulk modulus, and elastic constant of Ni_3Al agree with previous calculations and experiments.

3.1. Lattice constants

We have calculated the lattice constants of the γ, γ' phases with and without substitutional defects. Considering SOC as a "standard" calculation, non-spin and spin-polarized calculations exhibit different behaviors. SOC calculations give lattice constants of 3.518 Å and 3.567 Å for γ and γ' phases, respectively. The non-spin calculation gives a lattice vector that is 0.007 Å and 0.002 Å smaller for γ and γ', respectively. As shown in Fig. 2(a), spin polarized calculations give almost the same lattice parameters as SOC since the SOC effects are weak for light atoms. The spin polarized calculations are sufficient for Ni(γ) and Ni_3Al(γ') lattice relaxations. In Ni_3Al(γ'), for high density of Re-doped γ' ($1\times1\times1$ unit cell), non-spin introduces a difference of less than 0.1%; for the case of a low doping density ($2\times2\times2$ supercell), the difference is less than 0.03%, as shown in Fig. 2(b). Thus, spin and SOC effects are negligible when calculating lattice constants with a low doping density in Ni_3Al(γ').

Heavy-atom dopants enlarge the lattice of the γ' $2\times2\times2$ supercell by 0.01 Å to 0.06 Å as shown in supplementary material Table S2. Among Ta, W, and Re in the γ' system, due to the fact that the atomic radius of Ta is greater than that of W and Re, Ta has the biggest lattice at about 7.192 Å, which is 0.81% larger than the γ' supercell itself; W and Re enlarge the lattice by about 0.35%. The substitution of Ta_{Ni} increases the lattice constant by about 0.8% compared to the substitution of Ta_{Al}.

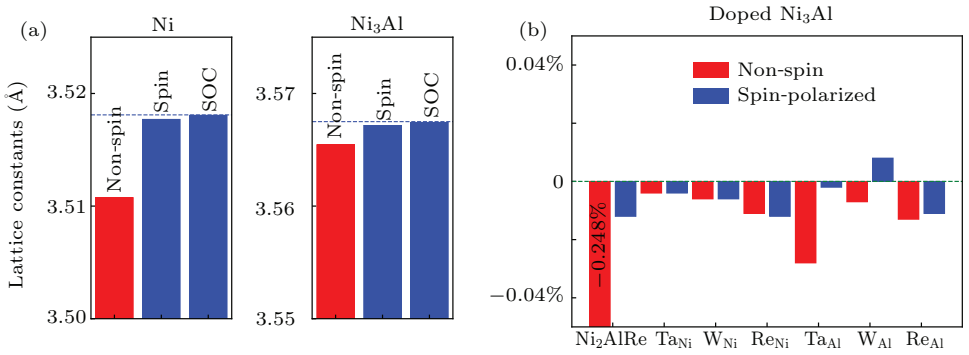


Fig. 2. Difference in lattice constants from non-spin, spin, and SOC calculations. (a) FCC-Ni and Ni_3Al lattice, (b) percentage difference of non-spin and spin lattice constant with respect to SOC calculations.

3.2. Bulk modulus

We have also calculated the bulk modulus of all the systems in the $2\times2\times2$ supercell. As shown in Fig. 3, non-spin and spin-polarized calculations often give larger values than SOC, except for Re_{Ni} in γ and γ'. Besides, non-spin calculations may introduce a variance of up to 5 GPa (3%) compared to SOC, but the value for spin-polarized cases is mainly around 1%. Interestingly, the Re atom in γ' results in an increase of bulk modulus of 6 to 7 GPa, showing that Re is more efficient than Ta and W in terms of increasing the bulk modulus.

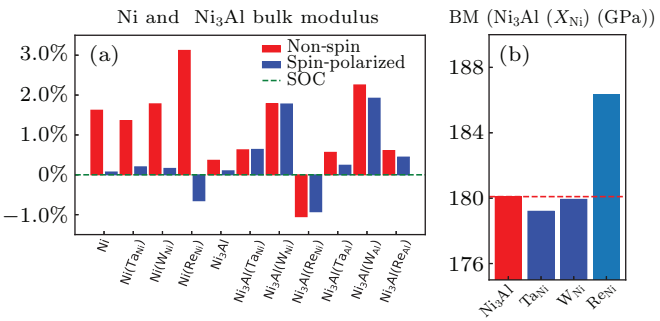


Fig. 3. Difference in bulk modulus from non-spin, spin and SOC calculations. (a) FCC-Ni and Ni_3Al bulk modulus, first four groups are Ni and Ni with defects in the γ phase, and others are Ni_3Al and Ni_3Al with defects in the γ' phase. (b) Bulk modulus of doped structures in the γ' phase with SOC, the Re-replacing-Ni case gives a larger bulk modulus (by about 6 GPa) than Re/W-replacing-Ni.

3.3. Formation energy

Formation energy is an important parameter to determine whether and where a dopant locates in superalloys. We have calculated the formation energy of Ta, W, and Re replacing Ni or Al in the γ' phase of a $2\times2\times2$ supercell at a doping density of 1/32. In Ni_3Al, it is found experimentally that substitutional Ta and Re atoms prefer to locate at Al sites,[10,13] which is consistent with our calculations (supplementary material Table S3). Our experimental results in the National Key

Research and Development Program also gave the same conclusion. As shown in Fig. 4, compared to the SOC calculated formation energy, non-spin calculations give a large difference (about 10 to 30%), and spin-polarized calculations improve the results, with differences of less than 10% with respect to SOC. Such difference implies that at doping density as low as 1/32, the SOC effects are still remarkable when calculating defect formation energy. For larger systems with several hundreds of atoms, we suggest that spin-polarized calculations should be performed.

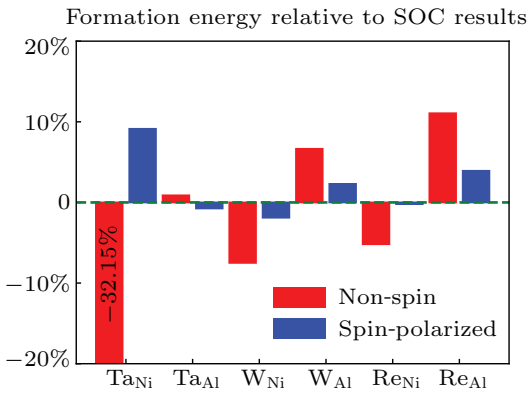


Fig. 4. Formation energies from non-spin, spin-polarized, and SOC calculations. The percentage is calculated with respect to SOC results of the supercells ($2 \times 2 \times 2$) of the γ' phase.

3.4. Elastic constant

To estimate the potential spin and SOC effects on the mechanical properties of superalloys, we have also calculated the elastic constant in the $2 \times 2 \times 2$ supercell of the γ' phase (C_{11} shown in Fig. 5 and C_{12} in supplementary material Table S5) considering spin and SOC effects and compared them with non-spin results. The trend is that, spin-polarized results are closer to SOC; however, as we increase the SOC strength manually to 200% and 300%, they approach the non-spin results again. The reason for this can be seen from the electronic calculations shown below, and we conclude that for large systems with several hundreds of atoms, the spin-polarized calculations should suffice.

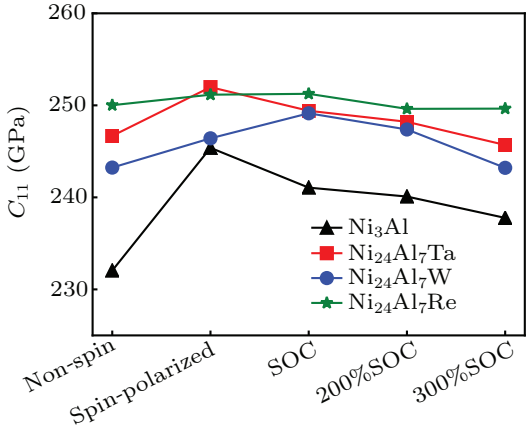


Fig. 5. Elastic constant C_{11} under non-spin, spin-polarized, and SOC calculations. The data are shown in supplementary material Table S4.

3.5. Electronic structure calculations

To investigate the mechanism of the overestimations of the bulk modulus, taking the Re doped $2 \times 2 \times 2$ Ni_3Al as an example, we performed differential charge density (DCD) calculations as shown in Fig. 6. The DCD represents the redistribution of charge density upon interactions between atoms, which is calculated as the following equation:

$$\rho = \Psi^*(\boldsymbol{r})\Psi(\boldsymbol{r}),$$
$$\rho_{\text{diff}} = \rho_{Ni_{24}Al_7Re} - \rho_{Ni_{24}Al_7} - \rho_{Re}.$$

Here, Ψ is the wavefunction in DFT calculations, and ρ is the density of electrons. Positive values (density of electrons increased) are colored in red, and negative values are in blue.

For the non-spin result, a significant charge transfer can be observed from the Ni atom to the doped Re atom, resulting in a strong dopant formation energy. By contrast, in the spin-polarized and the SOC results, the charge density, which comes from both Ni and Re atoms, aggregates between the two atoms, resulting in a relatively weak metallic bond. Thus, a relatively small bulk modulus should be observed, as shown in Fig. 3. The weakening of the metallic bond in the presence of SOC can be understood as follows. The d orbitals of the heavy doping atoms can give rise to an effective magnetic field that couples with the spin magnetic moment, i.e., $-\mu \cdot B$. Here, μ is the spin magnetic moment, and B is the magnetic field of the orbital moment. As a result, the spin polarization tends to align to the effective magnetic field. To form a chemical bond, it may cost additional energy to break the alignment comparing with the case without SOC. Despite of our simplified model, the argument of the softening of the chemical bond as well as the bulk modulus has its general validity in Re doped Ni_3Al system. For the typical concentration of the heavy doping atom, our results suggest that the SOC softens the chemical bond of its vicinity, giving a change in the bulk modulus. Of course, how strong SOC will affect the bulk modulus is dependent on the relative strength of the SOC compared to the crystalline electrostatic field and the dopant density.

We calculate the band structures of $2 \times 2 \times 2$ supercell ($Ni_{24}Al_7X$). Since the bands are folded in the Brillouin zone of the supercell, we perform a band unfolding calculation by vaspkit.[41] The unfolded non-spin, spin-polarized and SOC band structures of $Ni_{24}Al_7Re$, $Ni_{24}Al_7Ta$, and $Ni_{24}Al_7W$ are shown in supplementary material Figs. S1–S3. In Fig. 7, we take $Ni_{24}Al_7W$ as an example. We can see that the bands near Γ point and Fermi level are spilt in spin-polarized calculations, and the SOC effect tends to close the band gap of spin up and down, which causes the differences of the total energies in non-spin, spin-polarized, SOC calculations, and further varies the relevant properties.

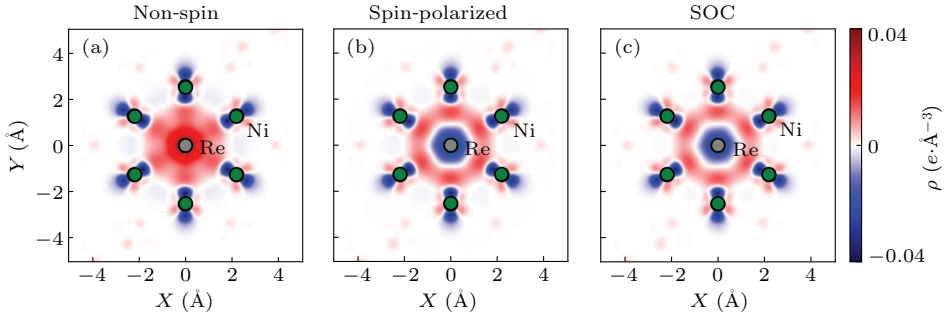


Fig. 6. Differential charge density analysis of $Ni_{24}Al_7Re$, from (a) non-spin, (b) spin-polarized and (c) SOC calculations, respectively. The electrons are transformed from the blue region to the red region. In contrast with the non-spin calculations, the spin-polarized and SOC ones have fewer electrons transforming from the Ni atoms to the Re atom, indicating the intensity of the metallic bonds is overestimated by the pure non-spin calculations. The reasons are discussed in the main text.

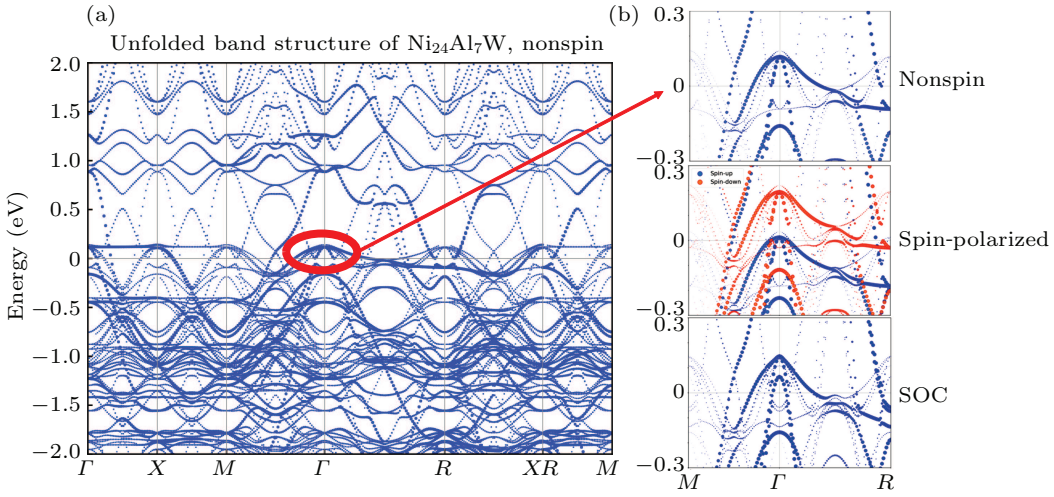


Fig. 7. (a) Unfolded band structure of $Ni_{24}A_7W$, non-spin calculation; (b) local zoom near Γ point and Fermi level of unfolded band structure. The scattering size indicates the weight of unfolded effective band structure in folded band structure.

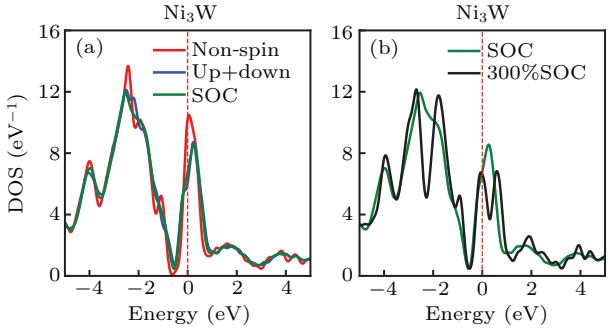


Fig. 8. Density of states by non-spin, spin, and different SOC strength calculations. The Fermi level has been set to 0. Here SOC300 means the SOC effects are artificially enhanced to 300%.

To highlight the SOC effect, we have also performed electronic structure calculations in the unit cell, using Ni_3W as an example for all the density of states (DOS), band structure, and magnetic moment calculations. Four types of calculations are performed, which are non-spin, spin-polarized, SOC and 300% SOC. DOS of Ni_3Re and Ni_3Ta are shown in the supplementary material. For the DOS shown in Fig. 8, non-spin, spin-polarized and SOC calculations agree with each other except for some energy ranges near the Fermi level. Besides, spin-polarized calculations cause a split near −2.5 eV due to the spin split on d band of Ni, according to the projected local DOS of d band shown in supplementary material Fig. S4. The t_{2g} orbitals cause the greatest effect at −2.5 eV; both t_{2g} and e_g orbitals split near the Fermi level due to the spin polarized effect, as show in supplementary material Fig. S7. Moreover, SOC effects on the d state of heavy metal further split the spin-up and spin-down states. This is more obvious for the calculations with 300%-SOC (see Fig. 8(b)). To understand the details, the band structures are analyzed.

In Fig. 9, the spin and SOC effects are shown to split the bands of the non-spin calculations, which is most obvious from path R to Γ. For bands dominated by the d state of heavy metal W, both spin-up and spin-down bands further split slightly due to the SOC effect, resulting in a decreased spin-up and spin-down separation in energy scale, and the magnetic moment of Ni_3W is decreased from $1.8\mu_B$ (spin-polarized result) to $1.3\mu_B$ (SOC result), and the stronger SOC (300% SOC) recreates degenerate states and causes the disappearance of the magnetic moment of the system. So, SOC effect tends to reduce the total magnetic moment of the alloys, as shown in Table 1. We can also find that the bands near the Fermi level of path X–M–R in non-spin calculation move upward and converge at the R-point in the 300% SOC strength calculation, contributing to the DOS peak-shift at the Fermi level shown in Fig. 8.

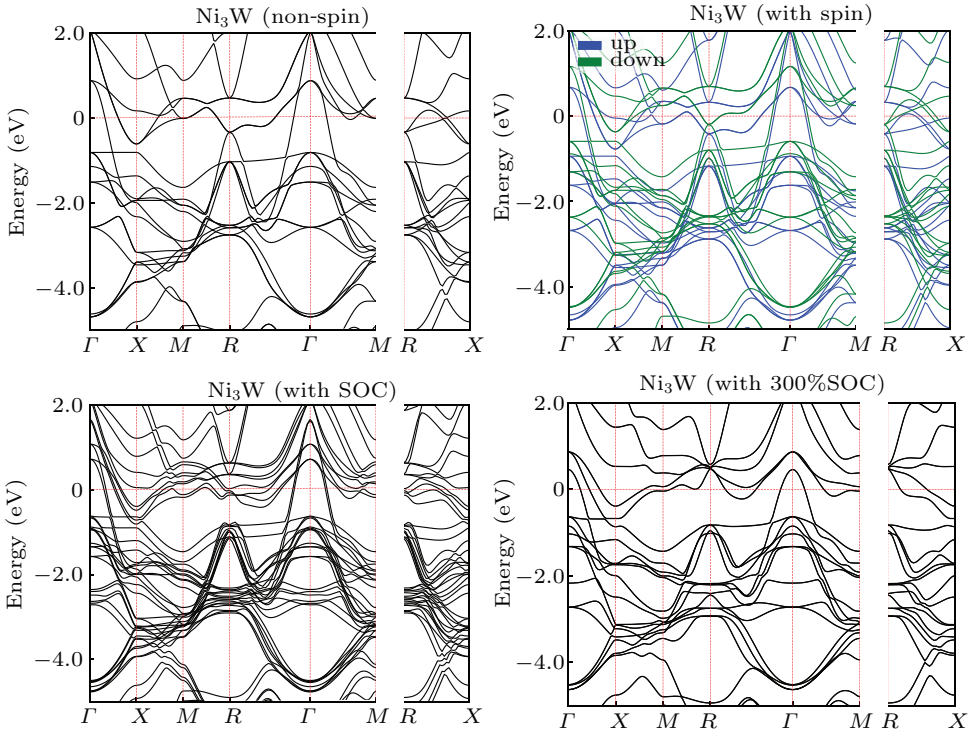


Fig. 9. Band structure of Ni_3W under different spin effects. The Fermi level has been set to zero. All of the high-symmetry lines are included in band-structure calculations, which follows the convention of AFLOWLIB.[42]

Table 1. Magnetic moments for Ni_3Re, Ni_3W, Ni_3Ta, $Ni_{24}Al_7Re$, $Ni_{24}Al_7Ta$, and $Ni_{24}Al_7W$ in units of μ_B.

	Spin	SOC	SOC 300%
Ni_3Re	2.2290	1.0350	0.0040
Ni_3Ta	0.2470	0.0510	0.0020
Ni_3W	1.8000	1.3280	0.0100
$Ni_{24}Al_7Re$	0.6795	0.6351	0.2494
$Ni_{24}Al_7Ta$	3.5557	3.7350	2.1564
$Ni_{24}Al_7W$	2.5272	2.1867	0.7089

4. Conclusion

The lattice constant, formation energy, mechanical properties, and electronic properties of γ, γ', and their Ta, W, and Re-doped alloys are calculated. Results under non-spin, spin-polarized, and SOC effects are compared. The lattice constant is not sensitive to the SOC effects and spin polarized calculations suffice for the γ phase. In the γ' phase, spin and SOC effects are negligible when calculating the lattice constant. For the bulk modulus, the difference can be between 1% and 3% without the SOC effect, and spin-polarized calculations can reduce the difference to 1%, so, we recommend including spin effect for both γ and γ' phases. Dopant formation energy is sensitive to different spin effects, even spin-polarized calculations give difference of between 1% and 9% at a doping density of 1/32, which make us aware of the difficulty of finding where heavy atoms are located in the γ and γ' phases. The SOC effects on the elastic constant are small, at less than 5% at 1/32 dopant density, for large systems, spin-polarized calculations should suffice. Magnetic moments are also affected by different strengths of SOC calculations: a high SOC strength decreases the total magnetic moments to a greater extent. Electronic structures calculations indicate that spin polarization causes a split in the metal d states, and SOC introduces a further split in the spin-up and spin-down states of the d states of heavy metals and reduces the magnetic moment of the system. To sum up, spin-polarized calculations suffice for most of the properties mentioned in this study except for dopant formation energies, which can be as large as a few percent at a 1/32 dopant density. This makes it difficult to predict the heavy metal distribution in superalloys, since including SOC effect in structural relaxation is quite expensive.

Acknowledgement

Project supported by the National Key Research and Development Program of China (Grant Nos. 2017YFB0701603 and 2017YFB0701502).

References

[1] Reed R C 2008 *The superalloys: fundamentals and applications* (Cambridge: Cambridge Univ. Press)
[2] Caron P and Khan T 1999 *Aerospace Science and Technology* **3** 513
[3] Betteridge W 1984 *Nickel and its alloys monographs in toxicology: Environmental and safety aspects* (New York: Halsted Press)
[4] Furrer D and Fecht H 1999 *JOM* **51** 14
[5] Zhu Z, Basoalto H, Warnken N and Reed R 2012 *Acta Materialia* **60** 4888
[6] Kovarik L, Unocic R R, Li J, Sarosi P, Shen C, Wang Y and Mills M J 2009 *Progress in Materials Science* **54** 839
[7] Zhang H, Zhang S, Cheng M and Li Z 2010 *Materials characterization* **61** 49
[8] Liang W, Jiang Y, He Y, Xu N, Zou J, Huang B, Liu C and others 2011 *Intermetallics* **19** 1759

[9] Hemker K, Mills M and Nix W 1991 *Acta metallurgica et materialia* **39** 1901

[10] Booth-Morrison C, Mao Z, Noebe R D and Seidman D N 2008 *Appl. Phys. Lett.* **93** 033103

[11] Lin H and Pope D P 1990 *Journal of Materials Research* **5** 763

[12] Garimella N, Ode M, Ikeda M, Murakami H and Sohn Y H 2008 *Intermetallics* **16** 1095

[13] Hattori M, Goto N, Murata Y, Koyama T and Morinaga M 2006 *Materials Transactions* **47** 331

[14] Chen C, Zhang L, Xin J, Wang Y, Du Y, Luo F, Zhang Z, Xu T and Long J 2015 *J. Alloys Compd.* **645** 259

[15] Garimella N, Ode M, Ikeda M, Murakami H and Sohn Y H 2009 *Journal of Phase Equilibria and Diffusion* **30** 246

[16] Mabruri E, Sakurai S, Murata Y, Koyama T and Morinaga M 2008 *Materials Transactions* **49** 1441

[17] Chiba A, Hanada S and Watanabe S 1992 *Materials Science and Engineering: A* 108

[18] Peng P, Soh A, Yang R and Hu Z 2006 *Computational Materials Science* **38** 354

[19] Zhang X and Wang C Y 2009 *Acta materialia* **57** 224

[20] Wang C and Wang C Y 2008 *Surface Science* **602** 2604

[21] Gong X F, Yang G X, Fu Y H, Xie Y Q, Zhuang J and Ning X J 2009 *Computational Materials Science* **47** 320

[22] Yu X X and Wang C Y 2012 *Materials Science and Engineering: A* **539** 38

[23] Kumar K, Sankarasubramanian R and Waghmare U V 2018 *Computational Materials Science* **150** 424

[24] Aguayo A, Mazin I and Singh D 2004 *Phys. Rev. Lett.* **92** 147201

[25] Kresse G and Hafner J 1994 *J. Phys.: Condens. Matter* **6** 8245

[26] Kresse G and Furthmüller J 1996 *Phys. Rev. B* **54** 11169

[27] Kresse G and Joubert D 1999 *Phys. Rev. B* **59** 1758

[28] Perdew J P, Burke K and Ernzerhof M 1996 *Phys. Rev. Lett.* **77** 3865

[29] Methfessel M and Paxton A T 1989 *Phys. Rev. B* **40** 3616

[30] Van Lenthe E, Baerends E J and Snijders J G 1993 *Journal of Chemical Physics* **99** 4597

[31] Griffiths D J and Schroeter D F 2018 *Introduction to quantum mechanics* (Cambridge University Press)

[32] Vinet P, Smith J R, Ferrante J and Rose J H 1987 *Phys. Rev. B* **35** 1945

[33] Birch F 1947 *Phys. Rev.* **71** 809

[34] Murnaghan F 1944 *Proc. Natl. Acad. Sci. USA* **30** 244

[35] Larsen A H, Mortensen J J, Blomqvist J, *et al*. 2017 *J. Phys.: Condens. Matter* **29** 273002

[36] Milstein F 1971 *Phys. Rev. B* **3** 1130

[37] Hartsuijker C and Welleman J W 2007 *Engineering mechanics. Vol. 2: Stresses, strains, displacements*, edn. (Dordrecht: Springer)

[38] Hill R 1952 *Proc. Phys. Soc. A* **65** 349

[39] Jiang C, Sordelet D J and Gleeson B 2006 *Acta Materialia* **54** 1147

[40] Ong S P, Richards W D, Jain A, Hautier G, Kocher M, Cholia S, Gunter D, Chevrier V L, Persson K A and Ceder G 2013 *Computational Materials Science* **68** 314

[41] Wang V, Xu N, Liu J C, Tang G and Geng W T 2021 *Computer Physics Communications* **267** 108033

[42] Setyawan W and Curtarolo S 2010 *Computational Materials Science* **49** 299